water

MDPI

Article

Dynamic Analysis in Surface Water Area and Its Driving Factors in Northeast China from 1988 to 2020

Wei Shan [1,2,3,*], Lisha Qiu [1], Ying Guo [1,2,3], Chengcheng Zhang [1,2,3] and Min Ma [1]

[1] Institute of Cold Regions Science and Engineering, Northeast Forestry University, Harbin 150040, China; lisa-qiu@nefu.edu.cn (L.Q.); samesongs@126.com (Y.G.); zhangchengcheng789@163.com (C.Z.); 1036998750@nefu.edu.cn (M.M.)
[2] Ministry of Education Observation and Research Station of Permafrost Geo-Environment System in Northeast China (MEORS-PGSNEC), Harbin 150040, China
[3] Collaborative Innovation Centre for Permafrost Environment and Road Construction and Maintenance in Northeast China (CIC-PERCM), Harbin 150040, China
* Correspondence: shanwei456@163.com

Abstract: The spatiotemporal changes in surface water area (SWA) in the basins of Northeast China have far-reaching impacts on their economic, agricultural, and social development and ecological sustainability. However, the long-term variation characteristics of water bodies in the Northeast basin and its main driving factors are still unclear. Based on the global surface water dataset, combined with the Meteorological and Vegetation Normalized Index (NDVI) datasets, this study used linear regression and correlation analysis to investigate the temporal and spatial variation characteristics of surface water in Northeast China and its driving factors from 1988 to 2020. The results show that (1) the seasonal surface water area (SSWA) and permanent surface water area (PSWA) in Northeast China increased at the rates of 58.408 km^2/ year and 169.897 km^2/ year, respectively, from 1988 to 2020. Taking 2000 as the node, PSWA and SSWA showed a trend of first decreasing and then increasing. (2) Changes in surface water types in each basin have significant space–time differences, and the transition between water bodies is dominated by the addition and reduction of seasonal water bodies. PSWA decreased significantly in western basins such as the Ulagai River Basin, the Otindag Desert, and the Liao River Basin, but increased significantly in the Songhua River Basin. (3) The driving forces of surface water change in different basins are different. Temperature and NDVI play a leading role in the change of SWA in the western arid region; permafrost degradation under the condition of air temperature rise is an indispensable factor affecting SWA change in the Argun River Basin; the eastern basin with a larger surface water area responded more strongly to changes in precipitation and evapotranspiration. Land-use conversion and water conservancy project construction were the main reasons for the increase of SWA in the Songhua River Basin under reduced precipitation. This research provides a reference for the in-depth study of the characteristics of surface water resources in Northeast China and has important practical significance for the scientific management of water resources in the basin.

Keywords: surface water area; spatiotemporal variation characteristics; remote sensing; driver factors; climate change; Northeast China

check for updates

Citation: Shan, W.; Qiu, L.; Guo, Y.; Zhang, C.; Ma, M. Dynamic Analysis in Surface Water Area and Its Driving Factors in Northeast China from 1988 to 2020. *Water* **2022**, *14*, 2296. https://doi.org/10.3390/w14152296

Academic Editors: Athanasios Loukas and Maria Mimikou

Received: 20 June 2022
Accepted: 21 July 2022
Published: 24 July 2022

Publisher's Note: MDPI stays neutral with regard to jurisdictional claims in published maps and institutional affiliations.

Copyright: © 2022 by the authors. Licensee MDPI, Basel, Switzerland. This article is an open access article distributed under the terms and conditions of the Creative Commons Attribution (CC BY) license (https://creativecommons.org/licenses/by/4.0/).

1. Introduction

Water resources are the foundation to support the sustainable development of society, economy, and the ecological environment, and an indispensable and important resource for human survival and development [1,2]. The spatiotemporal dynamic changes of surface water bodies such as lakes, reservoirs, and rivers are crucial to the development of terrestrial ecosystems and social economy [3–5]. In the past 100 years, under the influence of global climate change and human activities, surface water resources have generally faced such problems as total decline, water pollution, type conversion, area reduction, and unknown

water rights, while the water cycle and hydrodynamics of surface water have changed accordingly [6–8]. Different trends in surface water dynamics reflect direct and indirect human and natural drivers. Interconversion between water bodies is a necessary condition for understanding the spatial distribution and inundation variability of surface water, which can reflect droughts and floods, land-use transitions, and even current hydropolitics [9–11]. From 1984 to 2015, about 90,000 km^2 of permanent water bodies in the world disappeared, and more than 70% of the permanent water bodies' losses occurred in the Middle East and Central Asia. Climate change and human activities are considered major influencers of SWA [6,12].

Remote sensing technology has become an important tool for obtaining real-time dynamic information about large-scale surface water bodies. Compared with station observations, remote sensing technology provides accessible, high-resolution, and long-term availability of surface water extents at regional and global scales as indicators of changes in water resources [13]. The European Commission Joint Research Center (JRC) global surface water historical dataset based on Landsat satellite images provides statistical data on the extent and changes of global surface water and has been widely used in regional hydrology and water resource monitoring. Wu et al. used this dataset to quantify the dynamics of surface hydrological connectivity in a multi-lake system in the Momoge National Nature Reserve in Northeast China [14]. Zhu et al. combined the JRC dataset and digital elevation model (DEM) data to explore the impact of glacier meltwater on reservoir water storage in the Qinghai–Tibet Plateau Basin [15]. Based on this data, Wang et al. studied the temporal and spatial variation characteristics of surface water in China and its impact on desertification [16]. The convenience and easy availability of JRC data provide good data support for the above studies.

Northeast China is a major agricultural production area and also a flood-prone area. In recent years, with the rapid development of the social economy and the intensification of agricultural production, the consumption of water resources has also increased rapidly [17]. One of the fastest-warming regions in the world, the average annual temperature in Northeast China has risen at a rate of 0.3 °C/10 year in the past 50 years [18]. The climate has become warmer and drier and the river runoff has dropped significantly, further increasing the risk of drought [19–21]. At the same time, permafrost in high latitudes is also continuously degraded, which will have a significant impact on the hydrology, ecology, and economy of the region. Objective and quantitative evaluation of the dynamic changes of surface water in Northeast China and its driving factors will help the rational development and sustainable use of water resources in the region in the future, and it is of great significance for the study of countermeasures to adapt to climate change [13,22]. However, the current hydrological research in Northeast China is still based on station observations, and most of them are limited to the analysis of a single period and a single area [23–27]. In previous studies, there has been a lack of research on surface water changes in Northeast China in terms of basins, and the impact of climate and vegetation cover changes on changes in water resources in Northeast China has not been systematically evaluated.

Therefore, the main purpose of this study is to explore the spatiotemporal dynamics and driving forces of surface water at different scales in Northeast China. Based on the JRC historical dataset from 1988 to 2020, with the basin as the fundamental geospatial unit, the interannual variation trend of SWA in different periods and its dynamic transformation process were analyzed by linear regression and overlay analysis. Combined with meteorological data and vegetation data, the correlation between SWA, climate, and vegetation was analyzed, and the various characteristics and main driving factors of SWA were revealed from the watershed scale. This study is helpful to understand the long-term dynamic changes of surface water in the study area and promote the development of water resources management.

2. Materials and Methods

2.1. Study Area

Northeast China, including Eastern Inner Mongolia, Heilongjiang, Jilin, and Liaoning provinces, extends from 115°32′ E to 135°09′ E and 38°42′ N to 53°35′ N (Figure 1). The area is about 1.52 × 10^6 km^2 and the altitude is between −10~2691 m [19,28]. Characterized by "three plains and three mountains", the study area is surrounded by low and medium mountains in three directions: Changbai Mountain in the southeast, Greater Khingan Mountains in the northwest, and Lesser Khingan Mountains in the northeast. The Sonnen Plain, Liaohe Plain, and Sanjiang Plain are placed in the middle, south, and northeast, respectively. Hulunbuir Plateau is located at the western end, with hills and plateaus located between mountains and plains. The main vegetation types in the hills and mountains are cold temperate broad-leaved, mixed coniferous forest, and cold temperate coniferous forest [29], while semi-arid shrubs, grasslands, and temperate grasslands are dominant in the western region. Most of the study area has a temperate continental monsoon climate, and the continental climate gradually increases from east to west. The temperature gradually increases from north to south, with an annual average of −6 to 12 °C. The precipitation gradually decreases from east to west, between 1100~80 mm, with 70–80% of the precipitation concentrated from mid-June to mid-August [30,31]. The area with latitude >50° N is dominated by a cold monsoon climate. As the area with the highest latitude in China, the north of Yichun–Nenjiang is a permafrost area, and the south is a seasonally frozen soil area. The area of permafrost is about 0.38~0.39 × 10^6 km^2. Because it is placed in the degraded southern margin of the permafrost region of the Eurasian continent, the continuous warming of the climate will lead to the gradual degradation of the permafrost, and the degradation of the permafrost will directly affect the hydrological regime of the rivers [32,33].

The southern part of the study area is close to the Bohai Sea, and there are two major river basins: the Songhua River (5.5 × 10^5 km^2) and the Liaohe River (2.2 × 10^5 km^2) in the north and the south, the Argun River and some Inner Mongolia basins in the west, and the Wusuli River in the northeast [34]. The Songhua River is the largest tributary of Heilongjiang. It has two sources in the north and south. The north source is the Nenjiang River originating from the Yilehuli Mountain, a branch of the Greater Khingan Mountains, and the southern source is the Second Songhua River originating from Tianchi, Changbai Mountain. The Liaohe River is composed of two independent water systems: the East Liao Rivers and West Liao Rivers, bordering the Songhua River Basin in the north and Bohai Bay in the south. With the Greater Khingan Mountains as the boundary, the Argun River Basin is to the west of the Songhua River Basin, and the Hailar River originates from the west side of the Greater Khingan Mountains. The Argun River system in China mainly includes the Argun River, the Jiliu River, the Gen River, and the Hulun Lake. The southern part of the Argun River Basin is the Xilingol League of Inner Mongolia Autonomous Region. There are few drainage basins and little runoff. Except for the Luan River Basin in the east, which is an outflow water system, the rest of the water systems are inflow water systems, mainly including Dalinuoer, Ulagai River, and Chagannuoer Basin, with the south being the Otingag Desert. In this study, at different regional scales, using hydrology analysis according to the three-level watershed data, 12 representative watersheds were selected to analyze the spatiotemporal variation characteristics and main influencing factors of their surface water: Songhua River Basin and its tributaries: Nen River Basin and Second Songhua River Basin; Liao River Basin; Wusuli River Basin; Yalu River Basin; Argun River Basin and its two sub-basins: Gen River Basin and Hailar River Basin; Ulagai River Basin; Otindag Desert; and the Heilong River Basin in the northernmost part of China.

2.2. Data

2.2.1. Surface Water Data

In this study, the surface water data were obtained from the JRC yearly water history for the past 33 years (1988–2020), which was collected from Landsat 5, 7, and 8 satellite

images with a spatial resolution of 30 m. Visual analysis and evidence reasoning was used to separate each pixel as water/non-water (http://global-surface-water.appspot.com/download accessed on 25 December 2021). We selected band 2 "Seasonal water" and band 3 "Permanent water" in the year history data as the research data. The Transitions dataset provides information on seasonal changes between the first and last year and captures changes between non-water, seasonal, and permanent water. The dataset provides 10 categories of information. The categories that are mainly used in this study are "Permanent (P)", "New permanent (NP)", "Lost permanent (LP)", "Seasonal (S)", "New seasonal (NS)", "Lost seasonal (LS)", "Seasonal to permanent (S2P)", and "Permanent to seasonal (P2S)". The above datasets were accessed and batch-stitched and cropped through the public data directory of the Google Earth Engine (GEE). Finally, spatial–temporal distribution and category conversion information of seasonal water bodies and permanent water bodies in the three periods of 1988–1999, 2000–2020, and 1988–2020 were obtained.

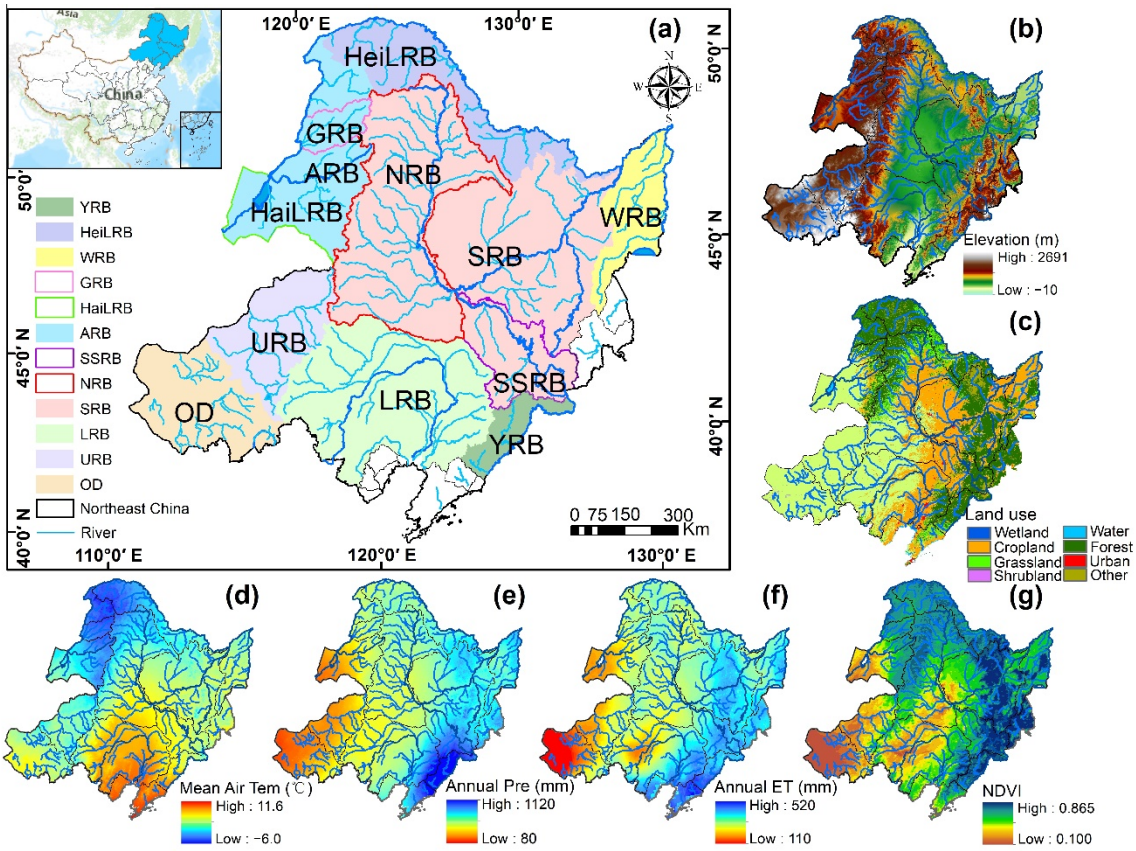


Figure 1. Spatial distribution of hydrology and driving factors in the study area. (**a**) Geographical location and watershed distribution of the study area. The main basins are: Yalu River Basin (YRB); Heilong River Basin (HeiLRB); Wusuli River Basin (WRB); Gen River Basin (GRB); Hailar River Basin (HaiLRB); Argun River Basin (ARB); Second Songhua River Basin (SSRB); Nen River Basin (NRB); Songhua River Basin (SRB); Liao River Basin (LRB); Ulagai River Basin (URB); Otindag Desert (OD). (**b**) Altitude, (**c**) land-use type, (**d**) mean air temperature, (**e**) annual precipitation, (**f**) annual evapotranspiration, and (**g**) NDVI.

2.2.2. Climate Data

All meteorological data used in this study were obtained from the National Tibetan Plateau Third Pole Environment Data Center (http://data.tpdc.ac.cn/zh-hans/ accessed on 5 January 2022). The temperature and precipitation data are a 1 km monthly dataset for China, which is based on the CRU global 0.5° climate dataset and the WorldClim global high-resolution climate dataset, generated by Delta spatial downscaling scheme. It was validated using data from 496 independent meteorological observation points [35–37]. The

evapotranspiration data comprise the terrestrial evapotranspiration dataset across China, and the dataset is the surface evapotranspiration product (v.1.5) established based on the complementary evapotranspiration method [38,39].

2.2.3. Vegetation Data

The NDVI dataset comes from the GIMMS NDVI3g dataset from 1988 to 2001 and the MODIS NDVI dataset from 2002 to 2020. GIMMS NDVI3g is from NASA's Goddard Space Flight Center (https://ecocast.arc.nasa accessed on 15 November 2021), which is retrieved from NOAA AVHRR satellite data with a spatial resolution of 8 km and the time resolution of 15 d. The MODIS NDVI dataset comes from the earth observing system of NASA, with a spatial resolution of 1 km. The maximum value synthesis (MVC) method is used to reduce the influence of the atmosphere on clouds and aerosols to obtain monthly NDVI data. All data were resampled to 1 km, and the pixels with NDVI < 0.1 were considered non-vegetation areas and filtered out.

2.2.4. Auxiliary Data

Additional auxiliary data include Shuttle Radar Topographic Mapping Mission (SRTM) DEM at 30 m resolution, obtained from the United States Geological Survey (USGS) (https://earthexplorer.usgs.gov/ accessed on 15 November 2021). The land-use data is the MCD12Q1 data product with a spatial resolution of 500 m in 2019. In addition, the river network data and the HydroBASINS data of the study area were obtained from the HydroSHEDS website to test the consistency of the watershed division (https://www.hydrosheds.org/ accessed on 25 December 2021).

2.3. Methods

Linear regression analysis reflects the linear relationship between a dependent variable and an independent variable. This study uses this method to calculate the rate of change of SWA, climatic factors, and NDVI. A positive slope indicates an increasing trend for the variable over time and a negative slope indicates a downward trend. Secondly, the statistical significance of the trend was calculated by the F test, and at the 95% and 99% significance levels ($p < 0.05$ and $p < 0.01$, respectively), it was tested whether the linear relationship was significant in general.

In addition, Pearson correlation analysis was used to explore the correlation between SWA and its driving factors [40]. The correlation coefficient formula is:

$$r_{xy} = \frac{\sum_{i=1}^{n}[(x-\overline{x})(y-\overline{y})]}{\sqrt{\sum_{i=1}^{n}(x-\overline{x})^2(y-\overline{y})^2}} \quad (1)$$

where n is the cumulative number of years in the monitoring period, x and y are the two samples of the correlation analysis, $\overline{x}$, $\overline{y}$ are the mean value of the variables, and r_{xy} is the correlation between the variable x and the variable y. The same significance test was carried out at the 95% and 99% significance levels ($p < 0.05$ and $p < 0.01$, respectively).

3. Results

3.1. Time Variation Trend of SWA in Northeast China

The trends of PSWA and SSWA in the three periods of 1988–2020, 1988–1999, and 2000–2020 were calculated (Figure 2). From 1988 to 2020, PSWA and SSWA showed an overall increasing trend. The mean value of PSWA is 21,123.56 km^2, with the maximum and minimum values in 1999 (24,087.54 km^2) and 1997 (16,548.77 km^2), respectively. PSWA increased at a rate of 58.408 km^2/year. It showed a decreasing trend before 2000 and increased at the rate of 174.504 km^2/year from 2000 to 2020. The mean value of SSWA is 17,306.12 km^2, with the maximum and minimum values in 2020 (29,707.17 km^2) and 1997 (9491.77 km^2), respectively. SSWA increased gently at a rate of 169.897 km^2/year (Figure 2b), but SSWA showed a fluctuating downward trend from 1988 to 1999, with a

change rate of −115.315 km^2/year. In addition, SSWA had two larger peaks in 1998 and 2013, which corresponded to two extreme precipitation events in the study area [41].

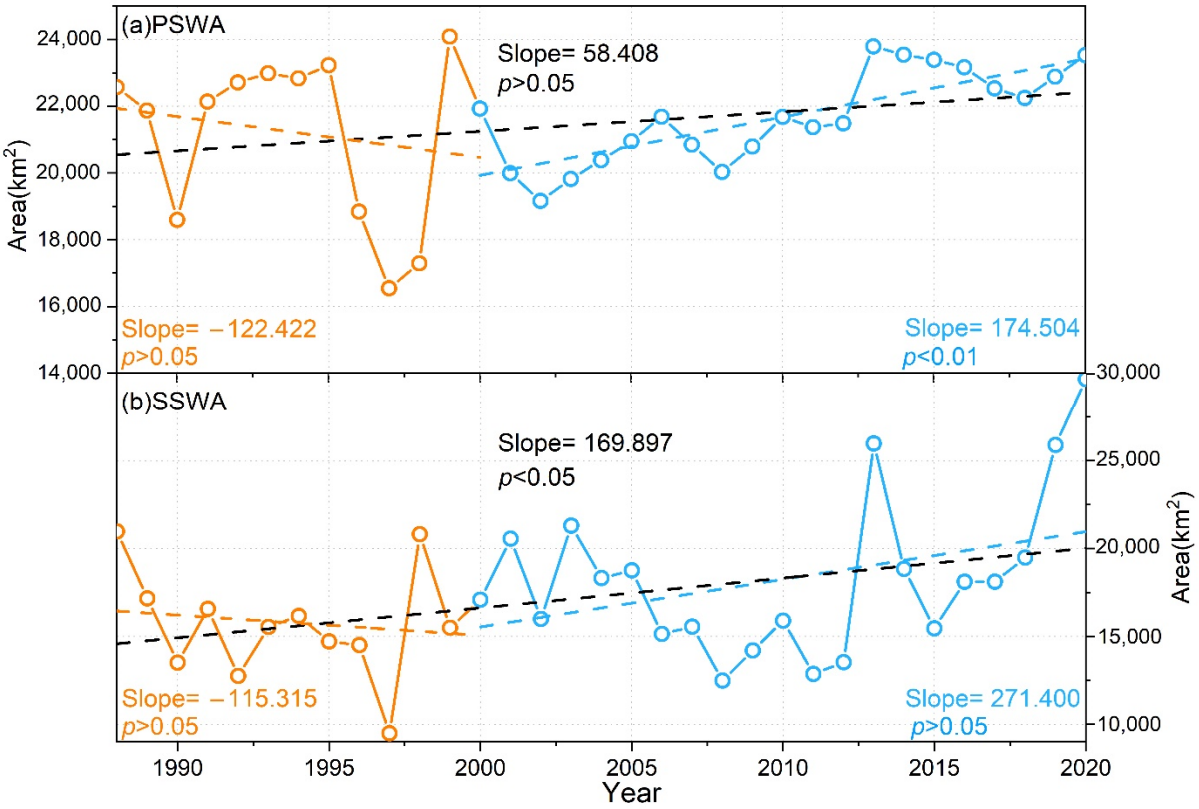


Figure 2. The changing trend of SWA. Due to the differences in data quality, using 2000 as the time node, the trend and significance of SSWA and PSWA in the three-time periods of 1988–1999, 2000–2020, and 1988–2020 were calculated, respectively. (**a**) PSWA, and (**b**) SSWA.

Further statistics on the variation trends of PSWA and SSWA in each basin in the three periods is shown in Figure 3. There are obvious spatial differences in the variation of SWA in the basins during the two periods of 1988–1999 and 2000–2020. From 1988 to 1999, SSWA and PSWA showed a trend of increasing in the west and decreasing in the east (Figure 3a,b). SSWA and PSWA in the Nen River Basin decreased at a rate of 167.360 km^2/year and 18.041 km^2/year, respectively, during this period. In the Second Songhua River Basin and Liao River Basin, SSWA increased significantly and PSWA decreased. From 2000 to 2020, the overall SWA in the basin showed an increasing trend. SSWA in the Hailar River Basin changed from increasing to an insignificant decrease, while the Nen River Basin changed from a significant decreasing trend to an insignificant increasing trend (Figure 3c). During the same period, the change of PSWA was mainly reflected in the reduction of the water area of the western basins. The PSWA of the Argun River Basin and Ulagai River Basin decreased significantly at the rate of 5.960 km^2/year and 14.431 km^2/year, respectively (Figure 3d).

From 1988 to 2020, the SWA of Songhua River Basin, Heilong River Basin, Wusuli River Basin, and Yalu River Basin mainly increased (Figure 3e,f). The SWA of the Liao River Basin shows a decreasing trend, and the decreasing rates of SSWA and PSWA were 1.453 km^2/year and 12.787 km^2/year, respectively. Changes in SWA in the Argun River Basin, Ulagai River Basin, and Otindag Desert are more complicated, with a significant increase in SSWA, while PSWA decreased at the rates of 9.438 km^2/year, 8.810 km^2/year, and 2.403 km^2/year, respectively. In most basins, the change rate of SSWA is large in the first stage, while the changing trend of PSWA is more significant in the second stage. The

overall change of SSWA is mainly affected by the period from 1988 to 1999, while PSWA is greatly affected by the period from 2000 to 2020.

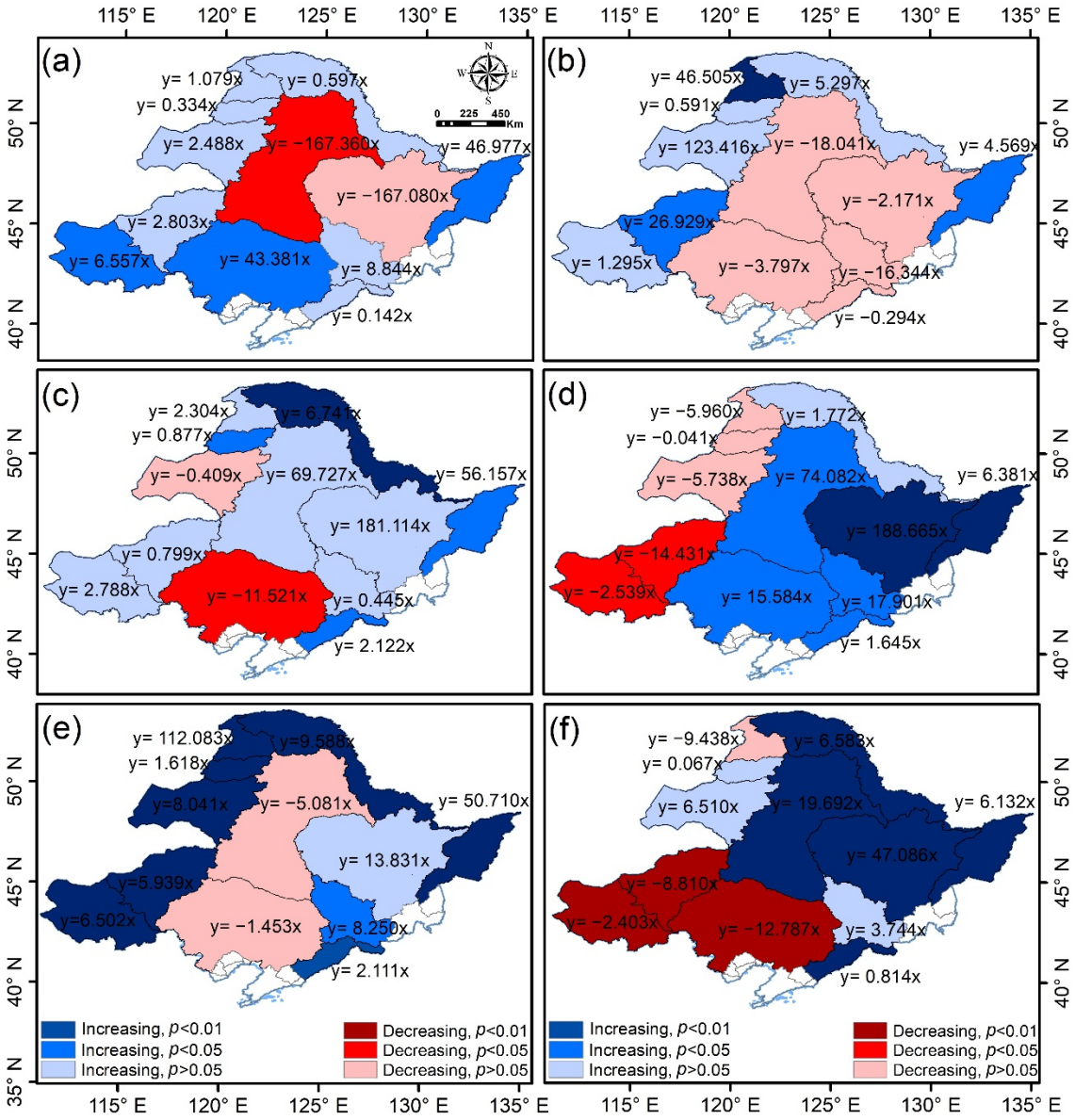


Figure 3. Interannual trends of SSWA and PSWA in the watershed: (**a**,**b**) are the trends of SSWA and PSWA for 1988–1999, respectively, (**c**,**d**) are the trends of SSWA and PSWA for 2000–2020, respectively, and (**e**,**f**) are the trends of SSWA and PSWA for 1988–2020, respectively.

3.2. Spatial Variation of SWA in Northeast China

Northeast China is rich in water resources, with rivers and reservoirs widely distributed in the study area (Figure 4). PSWA occupies 1.390% of the total area of the study area and these water bodies represent major rivers, large lakes, and reservoirs and are the main source of surface water. SSWA accounted for 1.139% of the total area of the study area. The main types of seasonal water bodies are streams, ponds, and the edges of large water bodies. The water area changes significantly with the seasons. In the rainy season, water bodies also exist in areas with shallow water levels, and seasonal water bodies reach a large area. In the dry season, the water body in this area may dry up, and the area of seasonal water bodies will be reduced accordingly. In relative terms, 87.591% of surface water is concentrated in the Songhua River Basin, Argun River Basin, and Liao River Basin, accounting for 65.223%, 13.321%, and 9.048% of the total, respectively. In the Argun

River Basin, Heilong River Basin, Second Songhua River Basin, Ulagai River Basin, and Yalu River Basin, the surface water is dominated by permanent water bodies, with PSWA accounting for more than 50% of the SWA in the basin. The permanent water bodies in the Argun River Basin, Second Songhua River Basin, and Ulagai River Basin account for 86.239%, 61.502%, and 59.955%, respectively (Table 1). The area difference between the two types of water bodies in the Liao River Basin and the Songhua River Basin is small. Gen River Basin, Wusuli River Basin, and the Otindag Desert are dominated by seasonal water bodies, which account for 80.256%, 70.125%, and 61.607%, respectively, of the SWA of the basin.

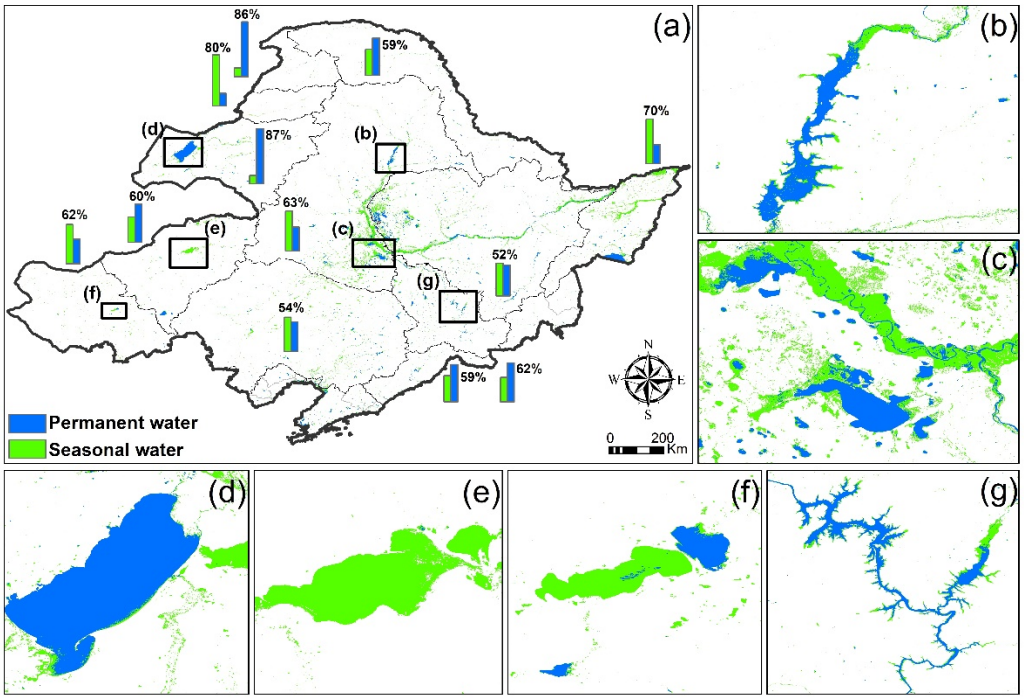


Figure 4. (**a**) The spatial distribution of surface water bodies and the proportion of SSWA and PSWA in Northeast China in 2020; (**b**–**g**) are Nierji Reservoir, Chagan Lake, Hulun Lake, Ulagai Lake, Chagannuoer, and Fengman Reservoir, respectively.

Table 1. Mean SWA values of watersheds for 1988–2020.

Basin	SSWA (km^2)	Percentage (%)	PSWA (km^2)	Percentage (%)	Total
ARB	642.663	13.761	4027.426	86.239	4670.089
GRB	37.375	80.256	9.195	19.744	46.57
OD	321.957	61.607	200.639	38.393	522.597
HaiLRB	586.752	13.003	3925.721	86.997	4512.473
HeiLRB	255.509	41.177	365.006	58.823	620.515
LRB	1697.865	53.528	1474.052	46.472	3171.917
NRB	4122.852	62.554	2468.060	37.446	6590.912
SRB	11,780.908	51.522	11,084.814	48.478	22,865.722
SSRB	824.059	38.498	1316.462	61.502	2140.521
URB	452.976	40.045	678.193	59.955	1131.168
WRB	1131.657	70.125	482.119	29.875	1613.776
YRB	190.199	41.150	272.012	58.850	462.211

Overall, the surface water in the study area is dominated by permanent water bodies, with PSWA 1.221 times that of SSWA. The PSWA of the Songhua River Basin was the largest, accounting for 52.476% of the total PSWA, while the Nen River Basin and Second Songhua River Basin accounted for 22.265% and 11.876% of its water area, respectively. The second

is Argun river basin, whose PSWA accounts for 19.066% of the total, of which 95.042% were distributed the in Hailar River Basin. More than two-thirds (68.074%) of the seasonal water bodies are concentrated in the Songhua River Basin, followed by the Wusuli River Basin and Argun River Basin.

The transitions between permanent water bodies, seasonal water bodies, and non-water at different times were analyzed (Figure 5). In the previous stage (1988–1999), the seasonal water bodies were mainly lost, with the newly added seasonal water bodies area (7096.162 km^2) smaller than the lost area (8993.969 km^2), so the overall seasonal water bodies decreased. In the latter stage (2000–2020), the area of seasonal water bodies increased significantly, while the area of seasonal water bodies converted to permanent water bodies also increased, with a converted area of 2881.8216 km^2. However, the area of permanent water loss in this stage is twice that of the first stage, so the area of new permanent water bodies in the second stage is slightly smaller than that in the first stage. In general, the study area from 1988 to 2020 was dominated by the addition of seasonal water bodies, and the area of various types of water bodies was: new seasonal > unchanged permanent > unchanged seasonal > new permanent > lost seasonal > seasonal to permanent > permanent to seasonal > lost permanent. The increased PSWA is 6489.213 km^2, with 29.826% of the newly added permanent water bodies converted from seasonal water bodies. The area of permanent water body reduction is 1520.561 km^2, of which 51.994% of this reduction is converted into seasonal water bodies. Newly added and completely lost areas of seasonal water bodies are 17,127.653 km^2 and 4143.395 km^2, respectively.

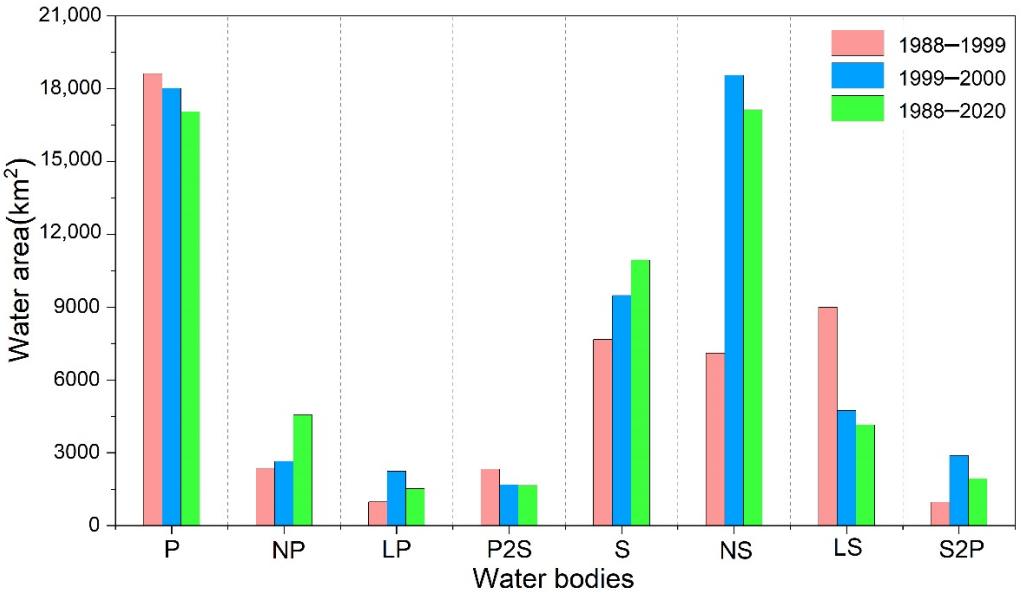


Figure 5. Transformation of surface water bodies in the study area for 1988–1999, 2000–2020, and 1988–2020. Among them, the conversion types are unchanged permanent (P), new permanent (NP), lost permanent (LP), permanent to seasonal (P2S), unchanged seasonal (S), new seasonal (NS), lost seasonal (LS), and seasonal to permanent (S2P).

In addition, the transformation of surface water bodies in each basin was compared during the three periods (Figure 6). From 1988 to 1999, the decrease in surface water mainly occurred in the Songhua River Basin, with the loss of seasonal water bodies 1.631 times that of the newly added seasonal water bodies. The main type was the conversion of seasonal water bodies to non-water bodies. Due to the large-scale drought in Northeast China in 1999 and 2000, many medium and small reservoirs dried up, the area of large reservoirs decreased, and the loss of SSWA was serious [42–44]. During the same period, the SWA of the Argun River Basin increased significantly, with new permanent and seasonal water bodies of 452.502 km^2 and 754.175 km^2, respectively. From 1998 to 1999, the area and number of lakes in Inner Mongolia increased sharply, with precipitation the main factor

affecting their changes during this period [45]. After 2000, the SWA of the Songhua River Basin increased significantly, with the seasonal and permanent water bodies increasing by 12,938.849 km^2 and 1788.862 km^2, respectively. In the west, the Argun River Basin, Ulagai River Basin, and Otindag Desert surface water loss is serious, and the Ulagai River Basin lost 628.103 km^2 of permanent water bodies. As drought intensifies, smaller lakes or ponds are more vulnerable than larger water bodies, so some smaller ponds and lakes dry up, resulting in a significant reduction in the area of permanent water bodies. In general, from 1988 to 2020, the change of surface water was mainly dominated by the conversion of seasonal water bodies, with the Songhua River Basin and Wusuli River Basin in the east mainly increased by seasonal water bodies and the arid areas in the west dominated by seasonal water body decreases. The increase of SWA in the study area was mainly influenced by large water bodies, while the decrease was mainly influenced by small water bodies.

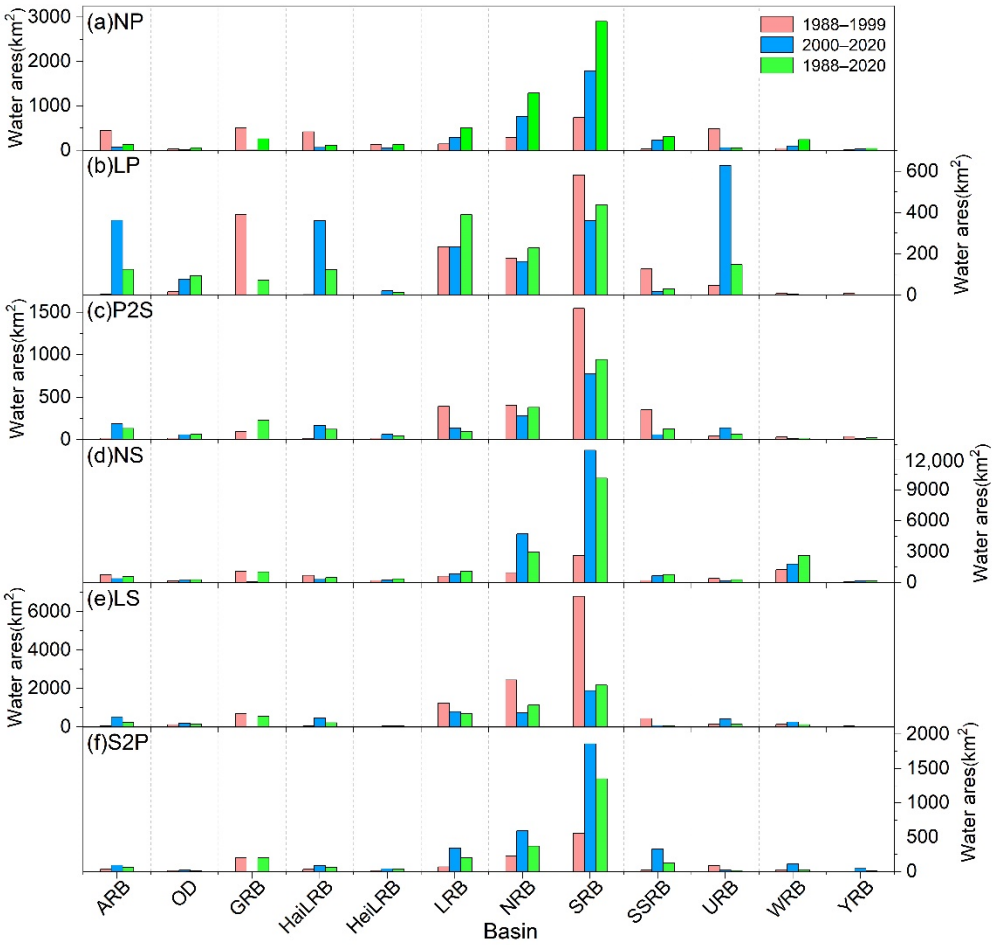


Figure 6. Conversion of surface water bodies in the basins: (**a**–**f**) are the areas of NP, LP, P2S, NS, LS, and S2P in the three-time periods of 1988–1999, 2000–2020, and 1988–2020 in each basin.

The spatial distribution of water bodies' conversion from 1988 to 2020 is shown in Figure 7. Unchanged permanent water bodies and seasonal water bodies are 17,044.832 km^2 and 10,932.640 km^2, respectively. It is worth noting that the contribution rate of seasonal water bodies to the newly added permanent water bodies is only 29.826%, so it is believed that the newly added permanent water bodies are greatly affected by human factors, such as the Naolong River Reservoir built in Nen River Basin in 1997 and the newly built water bodies in 2000. Shankou Reservoir (3745 km^2) and Nierji Reservoir (SWA over 400 km^2) were built in 2005 (Figure 7b,c). The construction of these medium and large reservoirs has greatly increased PSWA. The lost permanent water bodies and seasonal water bodies are mainly distributed in the west and northwest of the study area, such as Hulun Lake in

the Hailar River Basin (Figure 7d), Ulagai Lake in the Ulagai River Basin (Figure 7e), and Chagannuoer in the Otindag Desert (Figure 7f).

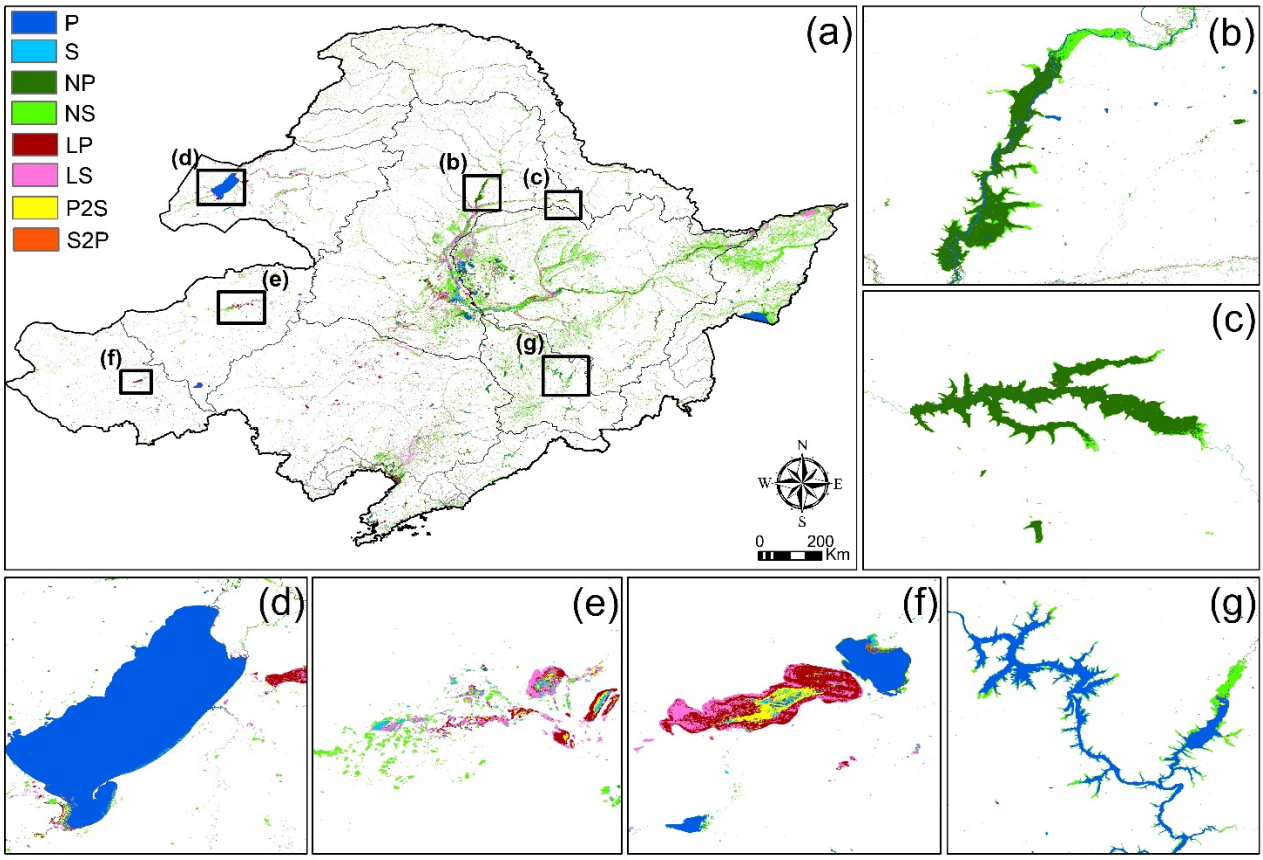


Figure 7. (**a**) Spatial pattern of surface water conversion in Northeast China for 1988–2020, and the water body conversion of (**b**) Nierji Reservoir, (**c**) Shankou Reservoir, (**d**) Hulun Lake, (**e**) Ulangai Lake, (**f**) Chagannuoer, and (**g**) Fengman Reservoir, respectively.

3.3. Correlation between NDVI and SWA

The correlations between SSWA, PSWA, and NDVI were significantly different in space (Figure 8). There was no significant negative correlation between SSWA and NDVI in the three periods of the Songhua River Basin and Ulagai River Basin ($p > 0.05$). There are certain differences on different time scales in the rest of the watersheds, with the Argun River Basin, Otindag Desert, and Wusuli River Basin having no significant positive correlation between SSWA and NDVI in the short-term (more than 10 years), but they have a very significant negative correlation in the long-term series (more than three decades). In the Heilong River Basin, Liao River Basin, and Yalu River Basin, SSWA was positively correlated with NDVI from 1988–1999 and negatively correlated after 2000–2020. Overall, SSWA and NDVI were mainly negatively correlated from 1988 to 2020. In the Heilong River Basin and Liao River Basin, SSWA and NDVI showed an extremely significant positive correlation (R = 0.443, $p < 0.01$) and insignificant positive correlation (R = 0.048, $p > 0.05$), respectively. In other watersheds, Songhua River Basin, Nen River Basin, Second Songhua River Basin, Gen River Basin, and Yalu River Basin were not significantly negatively correlated ($p > 0.05$), while SSWA of Argun River Basin, Ulagai River Basin, Otindag Desert, and Wusuli River Basin had an extremely significant negative correlation with NDVI ($p < 0.01$).

In contrast to SSWA, the correlation between PSWA and NDVI is mainly positive. The correlation between the Nen River Basin, Liao River Basin, and Ulagai River Basin was mainly positive in three periods, while PSWA and NDVI of the Hailar River Basin showed no significant negative correlation ($p < 0.05$). Overall, from 1988 to 2020, except

for the Gen River Basin, Hailar River Basin, and Yalu River Basin, PSWA was positively correlated with NDVI in other basins. The correlation between SWA and NDVI has obvious east–west differences between basins. For the Argun River Basin, Ulagai River Basin, and Otindag Desert in the western semi-arid region, SSWA and NDVI have a very significant negative correlation. In the Songhua River Basin and Liao River Basin with larger water areas in the eastern part of the study area, permanent surface water has a positive effect on vegetation development.

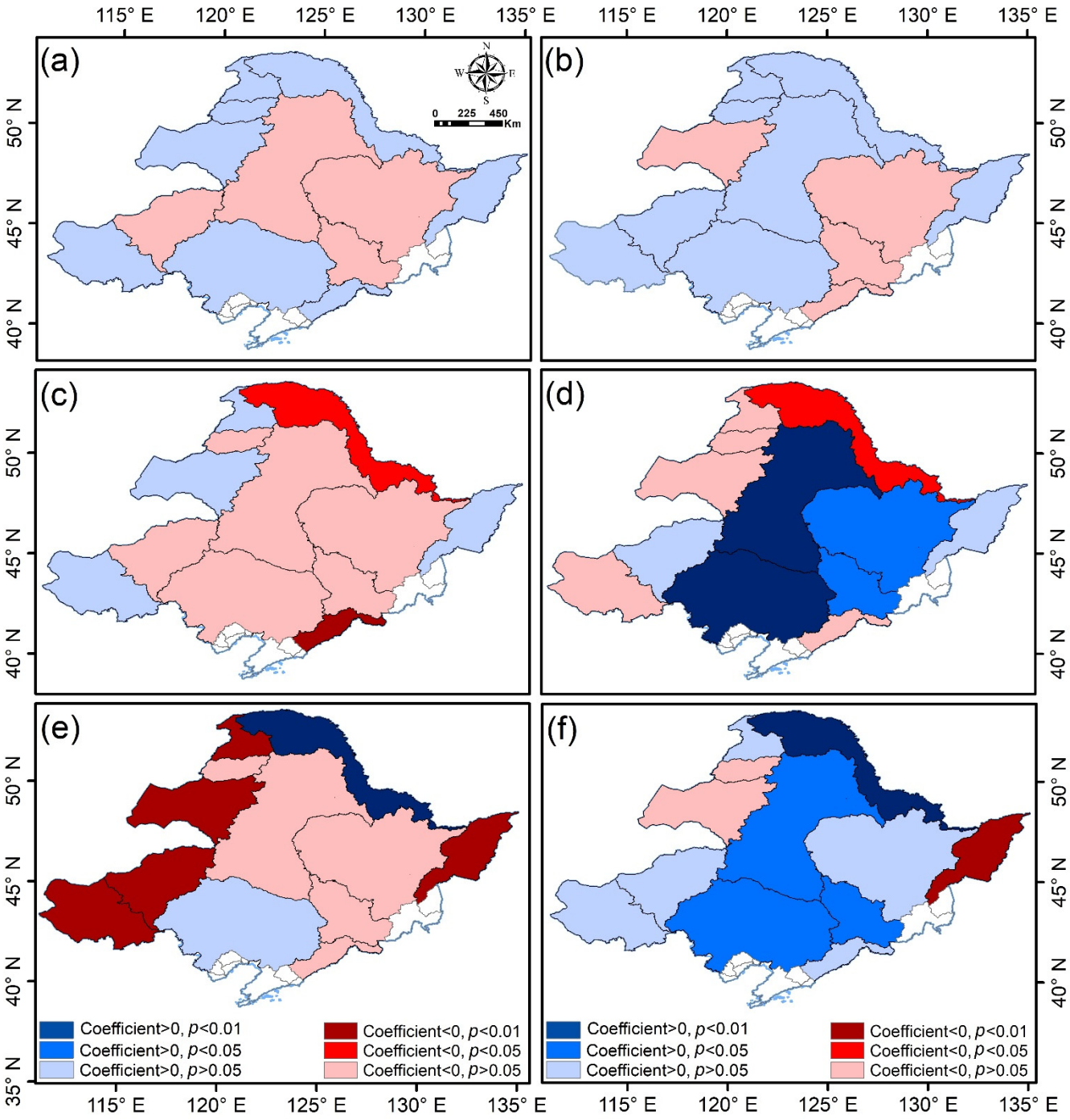


Figure 8. Spatial distribution of correlations of SSWA, PSWA, and NDVI in the watershed: (**a**,**b**) are the correlations of SSWA, PSWA, and NDVI for 1988–1999, (**c**,**d**) are for 2000–2020, and (**e**,**f**) are for 1988–2020.

3.4. Climate Drivers of Dynamic Changes in SWA

The Pearson correlation coefficients of SSWA with precipitation, temperature, and evapotranspiration were calculated (Figure 9). From 1988 to 1999, the correlation between SSWA and each climate driver was not significant due to the short time scale (Figure 9a). Precipitation, evapotranspiration, and SSWA were mainly positively correlated. Precipitation and SSWA showed an extremely significant positive correlation ($R = 0.712$, $p < 0.01$) and a significant positive correlation ($R = 0.540$, $p < 0.05$) in the Second Songhua River Basin and Yalu River Basin, respectively. From 2000 to 2020, the impact of precipitation on SSWA was enhanced, with the Gen River Basin ($R = 0.709$, $p < 0.01$), Nen River Basin ($R = 0.618$, $p < 0.01$), Songhua River Basin ($R = 0.478$, $p < 0.01$), and Wusuli River Basin ($R = 0.578$, $p < 0.01$) showing a very significant positive correlation (Figure 9b). In the long-term series (from 1988 to 2020), precipitation has the greatest impact on SSWA, followed by evapotranspiration. Three basins have extremely significant positive correlations with SSWA (Figure 9c). Temperature and SSWA were mainly positively correlated in each basin and were significantly positively correlated in the Ulagai River Basin, Wusuli River Basin, and Yalu River Basin (Figure 9).

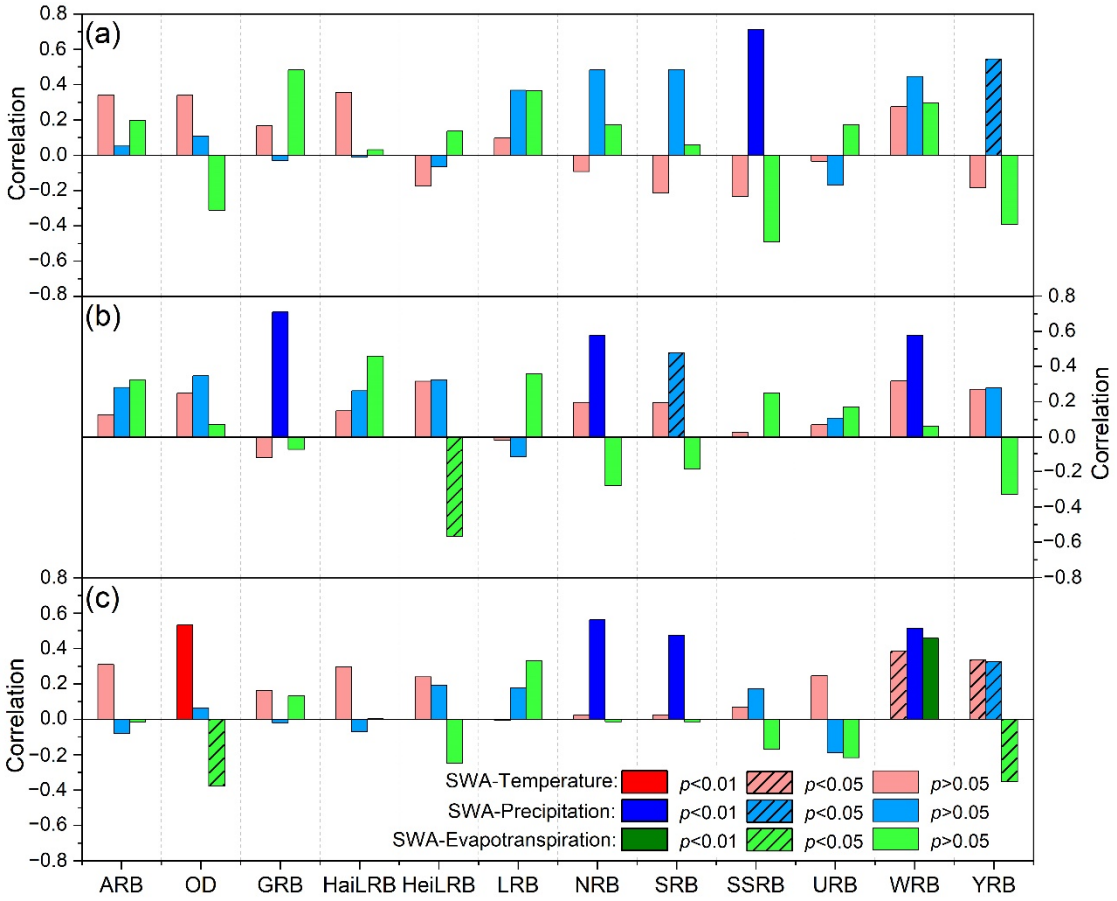


Figure 9. Correlations between SSWA and temperature, precipitation, and evapotranspiration in the basin at different times: (**a**) the correlation between SSWA and three climate factors for 1988–1999, (**b**) for 2000–2020, and (**c**) for 1988–2020.

Basin comparisons found that the main influencing factor of SSWA in the Argun River Basin, Hailar River Basin, and Gen River Basin was temperature. The temperature in the two periods of 1988–1999 and 1988–2020 was the most influential factor with the largest correlation coefficient. From 1988 to 2020, the Nen River Basin ($R = 0.563$, $p < 0.05$), Wusuli River Basin ($R = 0.513$, $p < 0.05$), Songhua River Basin ($R = 0.474$, $p < 0.05$), and other basins with large water areas and large flow were mainly affected by precipitation. The main

influencing factor of SSWA in the Heilong River Basin, Liao River Basin, and Yalu River Basin was evapotranspiration.

PSWA responds more strongly to the changes in precipitation and evapotranspiration (Figure 10). In 2000–2020 and 1988–2020, the precipitation of six and four basins, respectively, had a significant positive correlation with PSWA (Figure 10b,c). From 1988 to 2020, evapotranspiration was positively correlated with PSWA in the Liao River Basin (R = 0.486, $p < 0.01$), Ulagai River Basin (R = 0.445, $p < 0.01$), and Wusuli River Basin (R = 0.511, $p < 0.01$). There was no significant negative correlation between temperature and PSWA. The main driving factors of PSWA in the watershed were roughly the same as those of SSWA, but the temperature in the Gen River Basin, Ulagai River Basin, and Otindag Desert was positively correlated with SSWA and had a negative effect on PSWA.

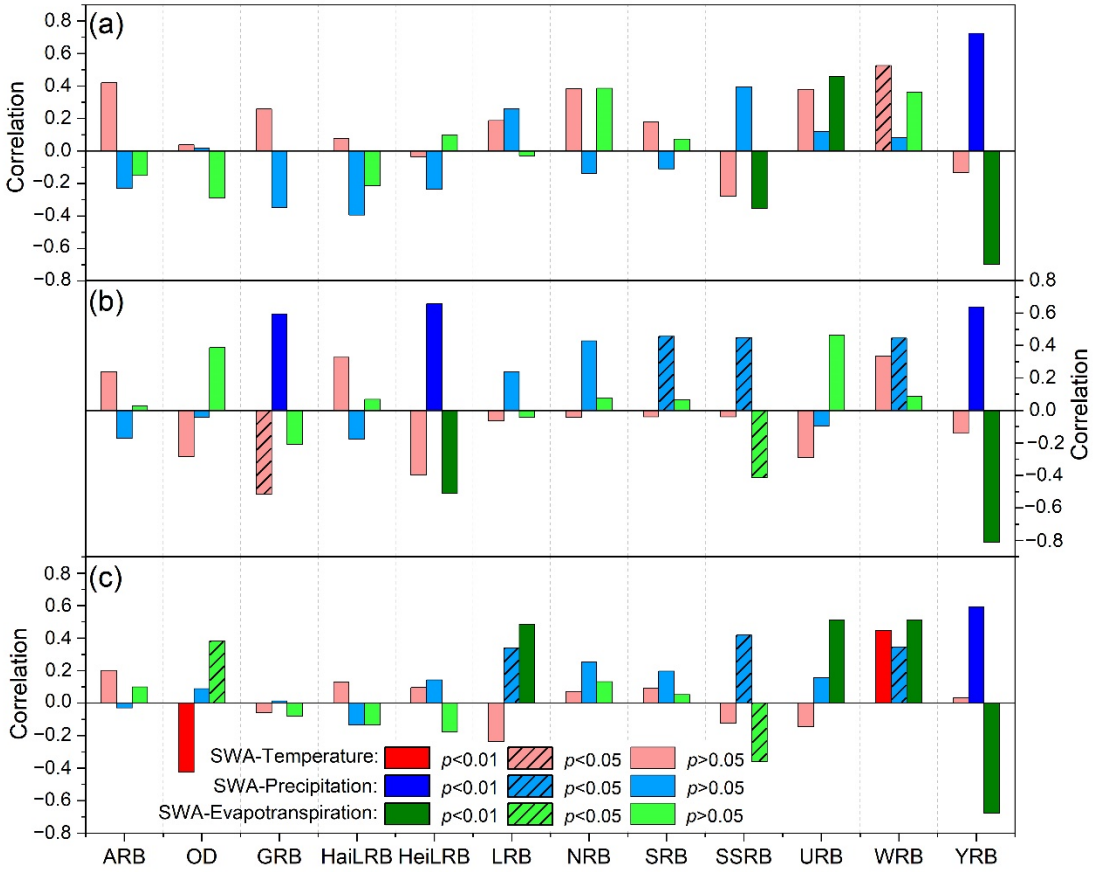


Figure 10. Correlations between PSWA and temperature, precipitation, and evapotranspiration in different periods: (**a**) the correlation between PSWA and three climate factors for 1988–1999, (**b**) for 2000–2020, and (**c**) for 1988–2020.

4. Discussion

4.1. Drivers of SWA Change

At the basin scale, the spatiotemporal dynamic characteristics of SWA in Northeast China were analyzed. The variation trends of SSWA and PSWA in each basin in the study area were significantly different in space. In the arid and semi-arid regions of the southwest, the SSWA of the Ulagai River Basin and the Otindag Desert showed a continuous upward trend, while PSWA showed an "up–down" trend, and the overall SWA declined significantly; The SWA of the Argun River Basin in the northwest also showed an "up–down" trend, but the overall trend was slightly increasing; The SWA in the central Songhua River Basin showed a trend of "decline–up", especially after 2000 when PSWA increased significantly. In addition, both SSWA and PSWA in the Liaohe River Basin showed a decreasing trend in recent years. To explain the difference in water body changes among

the basins, the relationship between SWA and air temperature, precipitation, and NDVI is analyzed, and the sub-basins can avoid the loss of some important spatial heterogeneity information. At the same time, the change rates of air temperature, precipitation, and NDVI in the basin were calculated to explore the main driving forces of SWA.

Ulagai River Basin and the Otindag Desert basins belong to arid and semi-arid areas, with drought and little rain throughout the year. PSWA showed a significant decreasing trend, but SSWA showed a significant increasing trend. In the past 33 years, the temperature of the Ulagai River Basin and Otindag Desert has increased significantly at the rate of 0.038 °C/year and 0.046 °C/year, respectively (Table 2). Although precipitation has increased after 2000, the overall climate still tends to be warm and dry. Temperature, NDVI, and SWA in the basin are well correlated. In the arid and semi-arid areas with scarce precipitation, with the temperature rise, most of the precipitation is consumed in the form of evapotranspiration, while vegetation transpiration consumes a lot of water, resulting in the low annual runoff coefficient of the basin [46]. Such climate-induced water stress may threaten forest and grassland growth. PSWA was positively correlated with NDVI ($R = 0.366$, $p < 0.01$), but the NDVI of the Ulagai River Basin and Otindag Desert decreased at a rate of 0.36×10^{-3}/year in the past 33 years (Table 2). Climate aridification and overgrazing may be the main factors leading to severe grassland degradation, which leads to the decline of grassland soil function, thus affecting the water resources supply, with SWA decreasing significantly [45].

The SSWA of the Argun River Basin shows a "rising–falling" trend, which is consistent with the previous runoff research results [26]. The correlation results of SWA, climate, and NDVI in this basin and its sub-basins are complex. The effect of temperature on PSWA is positive, but there is a negative correlation between precipitation and PSWA in the Gen River and Hailar River basins. In the Argun River Basin, besides the conventional climate and vegetation factors, the underlying surface factors such as permafrost should also be considered. As an important hydrological regulator of cold regions, warming-driven permafrost thawing and increased active layer thickness can alter river flow conditions in many ways [47]. During the thawing of permafrost from surface to deep, the surface runoff increased first and then decreased. The regression of permafrost in the early stage can directly increase runoff yield, but with the weakening of the water-retaining effect of the permafrost, more surface water in the basin is infiltrated into groundwater, which leads to the decrease of SWA in the basin [48]. The response of surface water in the basin to dynamic changes in permafrost requires further detailed discussion.

The SWA of the Songhua River Basin showed an overall increasing trend, while PSWA increased rapidly at the rate of 188.665 km^2/year from 2000 to 2020. Correlation analysis shows that precipitation is a major factor controlling surface water changes in the Songhua River Basin, and the correlation coefficients between precipitation and PSWA and SSWA from 2000 to 2020 are 0.456 ($p < 0.01$) and 0.478 ($p < 0.01$), respectively. However, the precipitation of the Songhua River Basin shows a slightly decreasing trend, while SWA increases significantly. Dong et al. believe that the decrease in precipitation but substantial increase of runoff in the basin is mainly affected by the change in various types of land cover. Since China entered the period of rapid economic development in 1980, a huge number of wetlands and woodlands have been reclaimed as cultivated land. After 2000, the water area in Northeast China decreased by 213.48 km^2 annually. A great number of beaches, lakes, and other water areas in the upper and middle reaches of the Songhua River Basin have been transferred to farmland. The original swamp supplies groundwater, and the stagnation, transpiration, and infiltration of forest land on surface water bodies are weakened; that is, the reduction of swamp and forest land has a positive effect on runoff and SWA [49–51]. In addition, the construction of water conservancy projects is another major factor in the dynamic changes of surface water. During the period from 1985 to 2015, the number of reservoirs in the area below the Sancha Estuary of the Songhua River in 2015 increased by 160% compared with 1985, while the area of reservoirs increased by 314%. The Nierji Reservoir, built in 2005, is a key project to solve the problem of the Liao River

Basin water shortage. It plays a key role in the regulation of Songhua River Basin and Liao River Basin water resources. It also makes the total area of the reservoir in 2005 about eight times that of 1985 [44,52].

Table 2. The trends of temperature (TMP, °C/year), precipitation (pre, mm/year), evapotranspiration (ET, mm/year), and NDVI (NDVI/year) in each basin of the study area during 1988–1999, 2000–2020, and 1988–2020.

Basin	Year	Linear Trend			
		TMP	PRE	ET	NDVI
ARB	1988–1999	0.096 *	−1.218	0.020	0.000
	2000–2020	0.035	3.618 **	−0.216 *	−0.001
	1988–2020	0.027 *	−0.900	−0.109 *	0.001 *
OD	1988–1999	0.101 **	0.816	−0.055	0.002
	2000–2020	0.029	2.648 *	−0.128	−0.001
	1988–2020	0.046 **	0.123	−0.125 **	−0.001
GRB	1988–1999	0.087 *	−0.910	0.148 *	0.001
	2000–2020	0.036	3.903 **	−0.237 *	−0.001
	1988–2020	0.026 *	−0.974	−0.034	0.002 *
HaiLRB	1988–1999	0.105 *	−1.491	−0.011	0.000
	2000–2020	0.033	3.620 *	−0.217 *	−0.001
	1988–2020	0.026 *	−0.981	−0.151 *	0.000
HeiLRB	1988–1999	0.043	−1.670	−0.003 *	0.002
	2000–2020	0.023	3.945 *	−0.18	−0.004
	1988–2020	0.018 *	0.864	−0.044 *	0.001
LRB	1988–1999	0.092 *	−2.362	−0.028	0.003 *
	2000–2020	0.025	4.675 **	−0.105	0.001 **
	1988–2020	0.028 *	−1.027	−0.182 *	0.002 *
NRB	1988–1999	0.090 *	−2.308	−0.034	0.001
	2000–2020	0.019	4.976 **	−0.091	0.001 **
	1988–1999	0.023 *	−0.638	−0.051 **	0.002 *
SRB	1988–1999	0.089 *	−3.745 **	−0.003	0.001 **
	2000–2020	0.019	5.723 *	−0.069	0.001
	1988–2020	0.024 *	−0.189	−0.052 *	0.002 *
SSRB	1988–1999	0.091 *	−5.980 **	0.005	0.001 *
	2000–2020	0.022	3.670	−0.017	−0.001
	1988–2020	0.026 *	−0.645	−0.010	0.002 *
URB	1988–1999	0.094 **	−0.003	−0.082	0.001
	2000–2020	0.030	3.078 *	−0.208	0.001
	1988–2020	0.038 **	−0.523	−0.233 **	−0.001 *
WRB	1988–1999	0.071 *	−1.449	0.115	0.001
	2000–2020	0.022	7.668 *	−0.019	−0.001
	1988–2020	0.022 *	2.264 *	0.128 *	0.001 *
YRB	1988–1999	0.073 **	−8.678	0.181 *	0.001
	2000–2020	0.027	1.535	−0.137	−0.003
	1988–2020	0.034 **	−0.442	−0.009	0.001

Note: * represents $p < 0.05$, ** represents $p < 0.01$.

4.2. Influence of Permafrost on SWA

The Argun River Basin is located on the southern margin of the permafrost region of the Eurasian continent. Due to the existence of permafrost on the underlying surface, the variation law of SWA in this region and its response to climate change is different from other basins. Changes in the active layer of permafrost affect surface runoff by changing the water storage capacity of the soil layer. Over the past 33 years, temperatures in the basin have risen significantly at a rate of 0.027 °C/year. From 1974 to 2006, the maximum

freezing depth of Manzhouli and Hailar decreased by 50 cm. After more than 30 years of degradation, the type of frozen soil has gradually changed from permafrost to seasonally frozen soil [53]. The influence of changes in the active layer and permafrost conditions on the hydrological cycle of the basin largely depends on the proportion of the permafrost area, permafrost temperature, and continuity [54]. The state and extent of permafrost are characterized by the area of frost number >0.5 [55], In terms of time series, the SSWA of the Argun River Basin is the same as that of permafrost, with a lag of one year in permafrost (Figure 11). The area with frost number >0.5 peaked in 2012, with the peak of SSWA occurring in 2013. There was no significant negative correlation between SSWA and the area with frost number >0.5. PSWA was significantly negatively correlated with the area with frost number >0.5 ($r = -0.567$, $p < 0.05$). In time series, the two showed opposite trends. When the area with frost number >0.5 in 2001, 2015, and 2018 was small, PSWA had a large value. In 2009 and 2012, the area with frost number >0.5 was at the peak, PSWA was at the trough, and SWA increased with the decrease of frozen soil area. Permafrost degradation often has lagged effects on seasonal runoff distribution [56], and soil thawing and freezing alter soil water storage capacity, infiltration capacity, and soil conductivity, redistributing water across soil profiles. Therefore, the seasonal variation of freeze–thaw in the active layer directly leads to the seasonal variation of groundwater flow, which affects the surface runoff process [57]. The runoff production process in the permafrost region has complex runoff recharge characteristics and influencing factors. In the future, further experiments will be needed to observe the relationship between the status of frozen soil and variables such as runoff and water area in the basin under climate change scenarios.

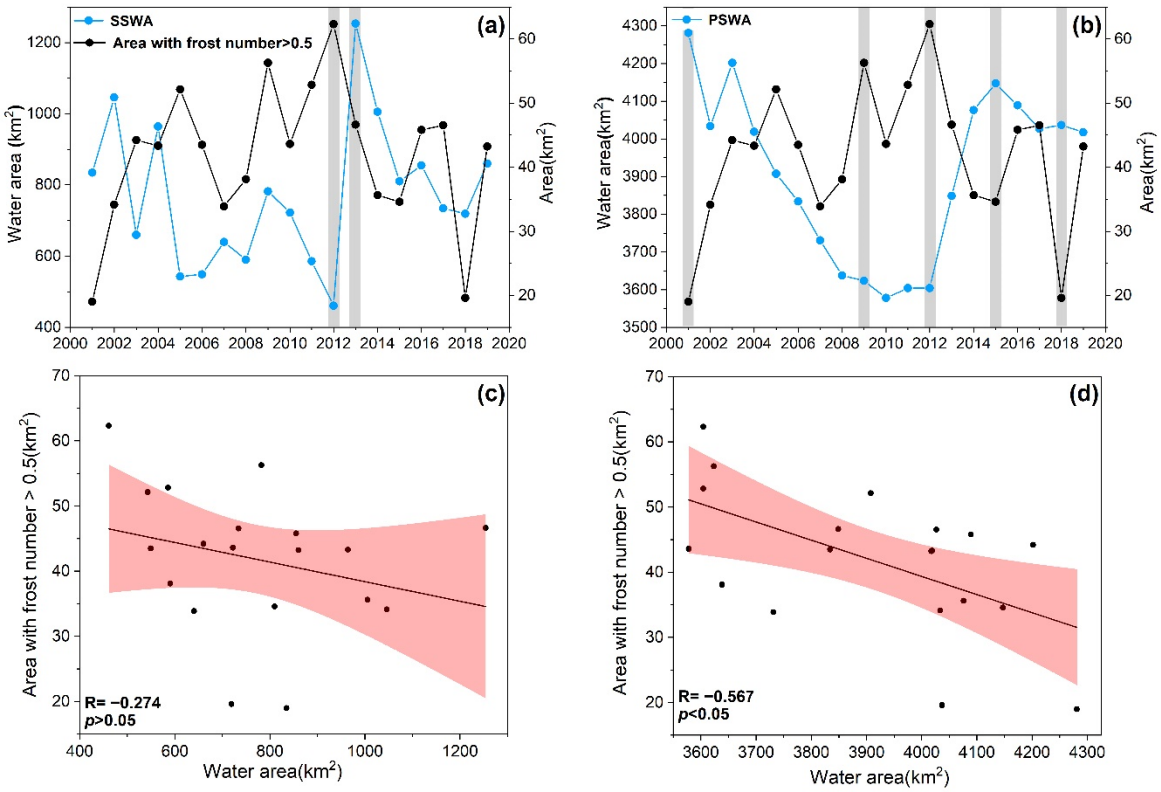


Figure 11. The interannual variation trend of SWA and the area with frost number >0.5 of the Argun River Basin and their correlation: (**a**,**b**) are the temporal changes of SSWA, PSWA, and the area of frost number >0.5, (**c**) is the correlation between SSWA and the area with frost number >0.5, and (**d**) is the correlation between PSWA and the area with frost number >0.5.

4.3. Research Uncertainty

In the JRC data, permanent water bodies refer to areas that are detected as water bodies throughout the year, and seasonal water bodies refer to areas with water bodies that

exist for less than 12 months in a year [6]. In this water extraction method, ice is regarded as an invalid observation, so the observation period only corresponds to the unfrozen months. Northeast China has a long freezing period within a year and solid water bodies cannot be monitored in winter. There are also certain errors in the observation of thin ice and snow during the thawing period in spring and the freezing period in early winter, making it difficult to observe the seasonal and periodic changes of water bodies in the study area during the year. In this study, only annual historical data are used to study the changes in SWA, and the water body transformation laws and driving factors in different river basins are explained from the macro level. The extraction of surface water ice should be considered in future research to obtain more accurate water extraction results and also study the seasonal variation characteristics of water bodies.

5. Conclusions

In this study, based on the global surface water area dataset from 1988 to 2020, combined with three climate factors of temperature, precipitation, evapotranspiration, and NDVI data, the spatiotemporal variation trends of SWA in Northeast China were systematically studied and the driving factors of surface water change in different periods were discussed at the watershed scale. The results of the study will contribute to future rational development and sustainable utilization of water resources in Northeast China. It is of great significance for the study of countermeasures to adapt to climate change.

From 1988 to 2020, the annual averages of PSWA and SSWA in Northeast China were 21,123.56 km^2 and 17,306.12 km^2, respectively, while SSWA and PSWA increased at a rate of 96.039 km^2/year and 121.386 km^2/year, respectively. The long-term variation of SWA in the watershed exhibits obvious spatial heterogeneity, with PSWA and SSWA showing a trend of first decreasing and then increasing. The largest change in SWA of the Songhua River Basin is also the most obvious, with SWA accounting for 52.476% of the total. The SSWA and PSWA of the Liao River Basin continued to decrease at the rate of 3.968 km^2/year and 11.024 km^2/year, respectively. The SSWA of the Argun River Basin, Ulagai River Basin, and Otindag Desert in the western part of the study area increased significantly, while PSWA decreased significantly.

The conversion between water bodies mainly occurred in seasonal water bodies. From 1988 to 2020, the conversion of water types was dominated by the increase of seasonal water bodies, with 51.994% of the reduced permanent water bodies converted into seasonal water bodies and 29.826% of the newly added permanent water bodies converted from seasonal water bodies. From 1988 to 1999, the loss of seasonal water bodies was relatively large. From 2000 to 2020, PSWA increased with the increase of the conversion of seasonal water bodies. The increase of SWA in the study area was mainly influenced by large water bodies, while the decrease was mainly influenced by small water bodies.

SSWA and NDVI are mainly negatively correlated, and NDVI is extremely significantly negatively correlated with SSWA in arid and semi-arid basins in the west in the long time series. PSWA and NDVI were mainly positively correlated and showed an extremely significant positive correlation in the Songhua River Basin and Liao River Basin with a large water area.

The driving factors of SWA change were significantly different in space. The climate factor affecting SWA in the western basin is temperature, while in the eastern basin it is precipitation. In the Ulagai River Basin and Otindag Desert, temperature, NDVI, and SWA were most correlated. The degradation of permafrost under climate warming may be an important factor affecting SWA changes in the Argun River Basin. Precipitation is the main factor controlling the change of SWA in the Songhua River Basin. The increase of SWA in the case of precipitation reduction is mainly affected by human activities such as land-use type transformation and water conservancy project construction.

Author Contributions: Conceptualization, W.S.; Data curation, W.S., L.Q., C.Z. and M.M.; Formal analysis, L.Q.; Funding acquisition, W.S.; Methodology, L.Q. and C.Z.; Project administration, W.S. and Y.G.; Resources, W.S.; Software, L.Q.; Writing—original draft preparation, W.S. and L.Q.;

Writing—review and editing, W.S., L.Q., Y.G., C.Z. and M.M. All authors have read and agreed to the published version of the manuscript.

Funding: We thank the National Natural Science Foundation of China (Grant No. 41641024) and Science and the Technology Project of Heilongjiang Communications Investment Group (Grant No. JT-100000-ZC-FW-2021-0182) for providing financial support and the Field scientific observation and research station of the Ministry of Education–Geological Environment System of Permafrost Area in Northeast China (MEORS-PGSNEC).

Institutional Review Board Statement: Not applicable.

Informed Consent Statement: Not applicable.

Data Availability Statement: Related data are available upon reasonable request.

Conflicts of Interest: The authors declare no conflict of interest.

References

1. Donchyts, G.; Baart, F.; Winsemius, H.; Gorelick, N.; Kwadijk, J.; Giesen, N. Earth's surface water change over the past 30 years. *Nat. Clim. Chang.* **2016**, *6*, 810–813. [CrossRef]
2. Mohammed, I.N.; Bolten, J.D.; Souter, N.J.; Shaad, K.; Vollmer, D. Diagnosing challenges and setting priorities for sustainable water resource management under climate change. *Sci. Rep.* **2022**, *12*, 1–15. [CrossRef] [PubMed]
3. Chen, J.; Kang, T.; Yang, S.; Bu, J.; Cao, K.; Gao, Y. Open-surface water bodies dynamics analysis in the Tarim River Basin (North-Western China), based on Google Earth Engine cloud platform. *Water* **2022**, *12*, 2822. [CrossRef]
4. Bo, Y.; Zhou, F.; Zhao, J.; Liu, J.; Liu, J.; Ciais, P.; Chen, L. Additional surface-water deficit to meet global universal water accessibility by 2030. *J. Clean. Prod.* **2021**, *320*, 128829. [CrossRef]
5. Jiang, Z.; Jiang, W.; Ling, Z.; Wang, X.; Peng, K.; Wang, C. Surface water extraction and dynamic analysis of baiyangdian lake based on the google earth engine platform using sentinel-1 for reporting sdg 6.6.1 indicators. *Water* **2021**, *13*, 138. [CrossRef]
6. Pekel, J.F.; Cottam, A.; Gorelick, N.; Belward, A.S. High-resolution mapping of global surface water and its long-term changes. *Nature* **2016**, *540*, 418–422. [CrossRef]
7. Deng, Y.; Jiang, W.; Tang, Z.; Ling, Z.; Wu, Z. Long-term changes of open-surface water bodies in the Yangtze River basin based on the Google Earth Engine cloud platform. *Remote Sens.* **2019**, *11*, 2213. [CrossRef]
8. Wang, R.; Xia, H.; Qin, Y.; Niu, W.; Pan, L.; Li, R.; Fu, P. Dynamic monitoring of surface water area during 1989–2019 in the hetao plain using landsat data in Google Earth Engine. *Water* **2020**, *12*, 3010. [CrossRef]
9. Hussein, H.; Grandi, M. Dynamic political contexts and power asymmetries: The cases of the Blue Nile and the Yarmouk Rivers. *Int. Environ. Agreem. Politics Law Econ.* **2017**, *17*, 795–814. [CrossRef]
10. Buerkert, A.; Schlecht, E. Rural–urban transformation: A key challenge of the 21st century. *Nutr. Cycl. Agroecosyst.* **2019**, *115*, 137–142. [CrossRef]
11. Riad, P.; Graefe, S.; Hussein, H.; Buerkert, A. Landscape transformation processes in two large and two small cities in Egypt and Jordan over the last five decades using remote sensing data. *Landsc. Urban Plan.* **2020**, *197*, 103766. [CrossRef]
12. Zhou, H.; Liu, S.; Hu, S.; Mo, X. Retrieving dynamics of the surface water extent in the upper reach of Yellow River. *Sci. Total Environ.* **2021**, *800*, 149348. [CrossRef] [PubMed]
13. Wang, M.; Du, L.; Ke, Y.; Huang, M.; Zhang, J.; Zhao, Y.; Gong, H. Impact of climate variabilities and human activities on surface water extents in reservoirs of Yongding River Basin, China, from 1985 to 2016 based on Landsat observations and time series analysis. *Remote Sens.* **2019**, *11*, 560. [CrossRef]
14. Wu, L.; Chen, Y.; Zhang, G.; Xu, Y.J.; Tan, Z. Integrating the JRC Monthly Water History Dataset and Geostatistical Analysis Approach to Quantify Surface Hydrological Connectivity Dynamics in an Ungauged Multi-Lake System. *Water* **2021**, *13*, 497. [CrossRef]
15. Zhu, J.; Song, C.; Ke, L.; Liu, K.; Chen, T. Remote Sensing Investigation of the Offset Effect between Reservoir Impoundment and Glacier Meltwater Supply in Tibetan Highland Catchment. *Water* **2021**, *13*, 1307. [CrossRef]
16. Wang, X.; Xiao, F.; Geng, X.; Hu, S.; Wang, Z. Spatiotemporal variations in surface water and its significance to desertification in China from 2000 to 2019. *CATENA* **2022**, *213*, 106182. [CrossRef]
17. Qi, W.; Feng, L.; Yang, H.; Liu, J. Spring and summer potential flood risk in Northeast China. *J. Hydrol. Reg. Stud.* **2021**, *38*, 100951. [CrossRef]
18. Liu, X.; Guo, Y.; Hu, H.; Sun, C.; Zhao, X.; Wei, C. Dynamics and controls of CO_2 and CH_4 emissions in the wetland of a montane permafrost region, northeast China. *Atmos. Environ.* **2015**, *122*, 454–462. [CrossRef]
19. Zhang, H.; Zhou, G.; Li Liu, D.; Wang, B.; Xiao, D.; He, L. Climate-associated rice yield change in the Northeast China Plain: A simulation analysis based on CMIP5 multi-model ensemble projection. *Sci. Total Environ.* **2019**, *666*, 126–138. [CrossRef]
20. Li, M.; Deng, G.; Shao, X.; Yin, Z.Y. Precipitation variation since 1748 CE in the central Lesser Khingan Mountains, Northeast China. *Ecol. Indic.* **2021**, *129*, 107969. [CrossRef]

21. Qi, W.; Feng, L.; Yang, H.; Liu, J. Warming winter, drying spring and shifting hydrological regimes in Northeast China under climate change. *J. Hydrol.* **2022**, *606*, 127390. [CrossRef]
22. Pickens, A.H.; Hansen, M.C.; Hancher, M.; Stehman, S.V.; Tyukavina, A.; Potapov, P.; Sherani, Z. Mapping and sampling to characterize global inland water dynamics from 1999 to 2018 with full Landsat time-series. *Remote Sens. Environ.* **2020**, *243*, 111792. [CrossRef]
23. Gu, R.Y.; Zhao, H.Y.; Li, C.; Meng, J. Characteristic of climate change in the ARgun drainage basin during 1960–2008. *J. Glaciol. Geocryol.* **2011**, *33*, 1310–1315. (In Chinese with English abstract)
24. Lu, Z.H.; Xia, Z.Q.; Yu, L.L.; Wang, J.C. Temporal and spatial variation of characteristics of precipitation in Songhua River Basin during 1958-2009. *J. Nat. Resour.* **2012**, *27*, 100–110. (In Chinese with English abstract)
25. Tu, G.; Li, S.F.; Sun, L.; Yao, Y.X. Temporal variation of observed runoff in Songhua River and Liaohe River Basins and its relationship with precipitation. *Adv. Clim. Chang. Res.* **2012**, *8*, 456–461. (In Chinese with English abstract)
26. Lu, Y.H.; Ye, B.S.; Li, C. Changes of runoff of the Hailar River basin in the southern margin of permafrost zone, Northeast China during 1958–2008. *J. Glaciol. Geocryol* **2014**, *36*, 394–402. (In Chinese with English abstract)
27. Yang, Z.; Gao, C.; Zang, S.; Yang, X. Applicability evaluation of the SWIM at river basins of the black soil region in Northeast China: A case study of the upper and middle Wuyuer River basin. *J. Geogr. Sci.* **2017**, *27*, 817–834. [CrossRef]
28. Mao, D.; Wang, Z.; Luo, L.; Ren, C. Integrating AVHRR and MODIS data to monitor NDVI changes and their relationships with climatic parameters in Northeast China. *Int. J. Appl. Earth Obs. Geoinf.* **2012**, *18*, 528–536. [CrossRef]
29. Shen, X.; Liu, B.; Xue, Z.; Jiang, M.; Lu, X.; Zhang, Q. Spatiotemporal variation in vegetation spring phenology and its response to climate change in freshwater marshes of Northeast China. *Sci. Total Environ.* **2019**, *666*, 1169–1177. [CrossRef]
30. Dang, Y.; Qin, L.; Huang, L.; Wang, J.; Li, B.; He, H. Water footprint of rain-fed maize in different growth stages and associated climatic driving forces in Northeast China. *Agric. Water Manag.* **2022**, *263*, 107463. [CrossRef]
31. Xiang, H.; Zhang, J.; Mao, D.; Wang, Z.; Qiu, Z.; Yan, H. Identifying spatial similarities and mismatches between supply and demand of ecosystem services for sustainable Northeast China. *Ecol. Indic.* **2022**, *134*, 108501. [CrossRef]
32. Gao, H.; Nie, N.; Zhang, W.; Chen, H. Monitoring the spatial distribution and changes in permafrost with passive microwave remote sensing. *ISPRS J. Photogramm. Remote Sens.* **2020**, *170*, 142–155. [CrossRef]
33. Shan, W.; Xu, Z.C.; Guo, Y.; Zhang, C.C.; Hu, Z.G.; Wang, Y. Geological methane emissions and wildfire risk in the degraded permafrost area of the Xiao Xing'an Mountains, China. *Sci. Rep.* **2020**, *10*, 1–21. [CrossRef] [PubMed]
34. Zhang, C.; Liu, Y.; Qiao, H. An empirical study on the spatial distribution of the population, economy and water resources in Northeast China. *Phys. Chem. Earth* **2015**, *79*, 93–99. [CrossRef]
35. Ding, Y.; Peng, S. Spatiotemporal trends and attribution of drought across China from 1901–2100. *Sustainability* **2020**, *12*, 477. [CrossRef]
36. Peng, S.; Ding, Y.; Liu, W.; Li, Z. 1 km monthly temperature and precipitation dataset for China from 1901 to 2017. *Earth Syst. Sci. Data* **2019**, *11*, 1931–1946. [CrossRef]
37. Peng, S.; Gang, C.; Cao, Y.; Chen, Y. Assessment of climate change trends over the Loess Plateau in China from 1901 to 2100. *Int. J. Climatol.* **2018**, *38*, 2250–2264. [CrossRef]
38. Ma, N.; Szilagyi, J.; Zhang, Y.; Liu, W. Complementary-relationship-based modeling of terrestrial evapotranspiration across China during 1982–2012: Validations and spatiotemporal analyses. *J. Geophys. Res. Atmos.* **2019**, *124*, 4326–4351. [CrossRef]
39. Ma, N.; Szilagyi, J. The CR of evaporation: A calibration-free diagnostic and benchmarking tool for large-scale terrestrial evapotranspiration modeling. *Water Resour. Res.* **2019**, *55*, 7246–7274. [CrossRef]
40. Chu, H.; Venevsky, S.; Wu, C.; Wang, M. NDVI-based vegetation dynamics and its response to climate changes at Amur-Heilongjiang River Basin from 1982 to 2015. *Sci. Total Environ.* **2019**, *650*, 2051–2062. [CrossRef]
41. Xu, J.A.; Li, X.H. Spatiotemporal evolution characteristics of extreme precipitation events in Northeastern China in recent 50 years. *Clim. Chang. Res. Lett.* **2021**, *10*, 352–364. (In Chinese with English abstract) [CrossRef]
42. Sun, L. Features of Weather/Climate over China in 1999. *Meteorol. Mon.* **2000**, *26*, 20–24. (In Chinese with English abstract)
43. Chen, Y. Features of Weather/Climate over China in 2000. *Meteorol. Mon.* **2001**, *27*, 20–24. (In Chinese with English abstract)
44. Hou, J.B.; Zheng, X.K.; Wang, M.; Wang, M.; Shang, Y.X.; Song, K.S. Remote sensing information extraction and pattern analysis of reservoirs in Northeast China. *Wetl. Sci.* **2017**, *15*, 582–587. (In Chinese with English abstract)
45. Zhou, Y.; Dong, J.; Xiao, X.; Liu, R.; Zou, Z.; Zhao, G.; Ge, Q. Continuous monitoring of lake dynamics on the Mongolian Plateau using all available Landsat imagery and Google Earth Engine. *Sci. Total Environ.* **2019**, *689*, 366–380. [CrossRef]
46. Zhang, J.A. Research on the Streamflow Responses to Climate Variability and Human Activities in Northeast China. Ph.D. Thesis, Dalian University of Technology, Dalian, China, 2013. (In Chinese with English abstract)
47. Song, C.; Wang, G.; Sun, X.; Hu, Z. River runoff components change variably and respond differently to climate change in the Eurasian Arctic and Qinghai-Tibet Plateau permafrost regions. *J. Hydrol.* **2021**, *601*, 126653. [CrossRef]
48. Tananaev, N.; Lotsari, E. Defrosting northern catchments: Fluvial effects of permafrost degradation. *Earth-Sci. Rev.* **2022**, *228*, 103996. [CrossRef]
49. Xu, D.X.; Zhang, G.X.; Feng, X.Q. Discussion on multiple time scales of runoff variation in the Nenjiang River Basin. *Resour. Sci.* **2009**, *31*, 1592–1598. (In Chinese with English abstract)
50. Xue, B.; Xiao, X.; Li, J.Z.; Xie, X.; Lu, C.P. Spatio-temporal evolution of water areas and croplands in the three provinces of Northeast China based on remote sensing data. *Chin. J. Ecol.* **2019**, *38*, 1444–1452. (In Chinese with English abstract)

51. Zhou, H.; Lei, G.P.; Yang, X.X.; Wang, T.T. Simulation of cultivated land under RCPs scenarios in typical basin of Sanjiang Plain. *Trans. Chin. Soc. Agric. Mach.* **2017**, *48*, 121–133. (In Chinese with English abstract)
52. Liu, Q.; Wang, Z.J.; Ma, T.M. The role Nierji hydraulic key project in the water resources adjustment and control of Nenjiang river basin. *J. Hydroelectr. Eng.* **2005**, *24*, 1–4. (In Chinese with English abstract)
53. Lu, Y.H.; Ye, B.S.; Li, C. Degradation of frozen ground in Hailaer River basin and its impact on hydrologic processes. *Adv. Water Sci.* **2013**, *24*, 319–325. (In Chinese with English abstract)
54. Wang, K.; Zhang, T.; Yang, D. Permafrost dynamics and their hydrologic impacts over the Russian Arctic drainage basin. *Adv. Clim. Chang. Res.* **2021**, *12*, 482–498. [CrossRef]
55. Nan, Z.T.; Li, X.X.; Cheng, G.D.; Huang, P.P. Surface frost number model and its application to the Tibetan Plateau. *J. Glaciol. Geocryol.* **2012**, *34*, 89–95. (In Chinese with English abstract)
56. Han, L.; Menzel, L. Hydrological variability in southern Siberia and the role of permafrost degradation. *J. Hydrol.* **2022**, *604*, 127203. [CrossRef]
57. Wang, G.; Hu, H.; Li, T. The influence of freeze–thaw cycles of active soil layer on surface runoff in a permafrost watershed. *J. Hydrol.* **2009**, *375*, 438–449. [CrossRef]